Published in final edited form as:
Bioconjug Chem. 2007 ; 18(5): 1498–1506. doi:10.1021/bc700184b.

A Macrophage—Nanozyme Delivery System for Parkinson's Disease

Elena V. Batrakova[*,†,‡], **Shu Li**[†,‡], **Ashley D. Reynolds**[§], **R. Lee Mosley**[§], **Tatiana K. Bronich**[†,‡], **Alexander V. Kabanov**[†,‡,⊥], and **Howard E. Gendelman**[†,§,‖]

Center for Drug Delivery and Nanomedicine, Department of Pharmaceutical Sciences, Center for Neurovirology and Neurodegenerative Disorders, and Department of Pharmacology and Experimental Neuroscience, University of Nebraska Medical Center, Omaha, Nebraska, and Department of Chemistry, M.V. Lomonosov Moscow State University, Moscow, Russia.

†*Center for Drug Delivery and Nanomedicine, University of Nebraska Medical Center*

‡*Department of Pharmaceutical Sciences, University of Nebraska Medical Center.*

§*Center for Neurovirology and Neurodegenerative Disorders, University of Nebraska Medical Center.*

‖*Department of Pharmacology and Experimental Neuroscience, University of Nebraska Medical Center.*

⊥*M.V. Lomonosov Moscow State University.*

Abstract

Selective delivery of antioxidants to the substantia nigra pars compacta (SNpc) during Parkinson's disease (PD) can potentially attenuate oxidative stress and as such increase survival of dopaminergic neurons. To this end, we developed a bone-marrow-derived macrophage (BMM) system to deliver catalase to PD-affected brain regions in an animal model of human disease. To preclude BMM-mediated enzyme degradation, catalase was packaged into a block ionomer complex with a cationic block copolymer, polyethyleneimine-poly(ethylene glycol) (PEI-PEG). The self-assembled catalase/PEI-PEG complexes, "nanozymes", were ca. 60 to 100 nm in size, stable in pH and ionic strength, and retained antioxidant activities. Cytotoxicity was negligible over a range of physiologic nanozyme concentrations. Nanozyme particles were rapidly, 40–60 min, taken up by BMM, retained catalytic activity, and released in active form for greater than 24 h. In contrast, "naked" catalase was rapidly degraded. The released enzyme decomposed microglial hydrogen peroxide following nitrated alpha-synuclein or tumor necrosis factor alpha activation. Following adoptive transfer of nanozyme-loaded BMM to 1-methyl 4-phenyl 1,2,3,6-tetrahydropyridine-intoxicated mice, ca. 0.6% of the injected dose were found in brain. We conclude that cell-mediated delivery of nanozymes can reduce oxidative stress in laboratory and animal models of PD.

INTRODUCTION

The need for delivery of therapeutic polypeptides to affected brain tissues in Alzheimer's and Parkinson's diseases, AD and PD) (1-3), infectious (meningitis, encephalitis, prion disease, and HIV-related dementia) (4,5), stroke (6,7), lysosomal storage (8,9), obesity (10,11), and

*Corresponding author. Tel: (402) 559-9364; fax (402) 559-9365; E-mail: ebatrako@unmc.edu..

Supporting Information Available: Experimental results of (1) enzymatic activity of catalase in polyion complexes, (2) cytotoxicity of nanozyme in BMM, (3) triggered release of catalase from BMM in the media, and (4) modulation of microglial-derived ROS by media collected from BMM loaded with PEI-PEG. This material is available free of charge via the Internet at http://pubs.acs.org.

other metabolic and inflammatory diseases of the central nervous system (CNS) is of immediate need and cannot be overstated.

An important component of metabolic and degenerative diseases of the nervous system involves inflammation (12). Such inflammatory activities are profound, as they lead to excessive production of pro-inflammatory products and reactive oxygen species (ROS) that lead in part, to cell death and neurodegen-eration. We posit that by affecting neuroinflammatory activities during disease, such as through the use of targeted antioxidants or drugs that inhibit the production or formation of pro-inflammatory cytokines and eicosanoids, the levels of ROS as well as other neurotoxins could be reduced, resulting in improved disease outcomes (13). However, such approaches have been limited, as drugs must not only penetrate the BBB but also find themselves in sufficient concentrations to affect ongoing disease mechanisms. Moreover, as inflammatory mechanisms are a likely early event for disease, therapeutic modalities must be used early and frequently. The limitation of drug delivery is one major obstacle confronting the development of new treatment paradigms for nervous system disorders.

One such disease is PD, the second most prevalent neurodegenerative disorder in people over 65. This disease is characterized by lack of the neurotransmitter dopamine due to a loss of dopaminergic neurons within the SNpc and their innervations to the striatum. PD neuropathology involves brain inflammation, microglia activation, and subsequent secretory neurotoxic activities, including ROS production, that play crucial roles in cell damage and death (14-17). PD brains show reduced levels of antioxidant enzymes and antioxidants (18-20) resulting in a reduced capacity to manage oxidative stress and associated neurodegeneration. Mounting evidence supports the notion that antioxidants can inhibit inflammatory responses and protect dopaminergic neurons in laboratory and animal models of PD (21-27). Catalase catalyzes the conversion of hydrogen peroxide, a known ROS, to water and molecular oxygen with one of the highest turnover rates for all known enzymes. In an *in Vitro* model of PD, catalase was shown to rescue primary cultured cerebellar granule cells from ROS toxic effects (13,28). Furthermore, a low molecular mass catalase activator, rasagiline, induced neuroprotection in a mouse model of PD (29). Few clinical trials have been performed using low molecular mass antioxidants, of which the most extensive used is α-tocopherol and deprenyl to inhibit the rate of PD progression (30). However, and as described above, most of the trials failed to show significant improvements because of restricted transport of α-tocopherol across the blood—brain barrier (BBB) and the time following the disease the drugs were used (31).

Recent works from our laboratories demonstrate that bone-marrow derived monocytes (BMM) can be used as carriers of nanoformulated drugs, both in the periphery and across the BBB (32,33). Entry into the brain occurs as a consequence of the establishment of a chemokine gradient induced through neuroinflammatory responses (34,35). Thus, we have sought to develop replicate PD-like model systems for testing the utility of cell-based delivery. First, divergent inflammatory cues were used to stimulate ROS production from microglia and included nitrated alpha synuclein (N-α-syn), thought to be released extracellularly in PD and elicit immune activation (36-38). Second, 1-methyl-4-phenyl-1,2,3,6-tetrahydropyridine (MPTP)-induced inflammation served as a gradient for BMM ingress into the brain. It is well-documented that following inflammatory cues, leukocytes are recruited to the brain through diapedesis and chemotaxis (39-43). Monocyte-macrophages can migrate across the brain paracellular spaces crossing junctional complexes of brain endothelial cells (44,45). Their combat arsenal consists of engulfing foreign particles and liberating engulfed substances by exocytosis. All together, these features make it possible to exploit macrophages as carriers to affect neuroinflammatory processes (46-49).

Here we used BMM as a vehicle for carriage of therapeutic concentrations of catalase to the brain. We found that a major obstacle for success in this approach is that macrophages efficiently disintegrate engulfed particles (49). Therefore, it is crucial to protect the activity of the enzyme inside of the cell-carrier. Incorporation into polymeric nanocarries (nanospheres, liposomes, micelles, nanoparticles) can provide such protection (50-60). Early work by V.A. Kabanov et al. demonstrated that use of interpolyelectrolyte complexes can immobilize enzymes (61-63). The enzyme polyelectrolyte complexes can be prepared at the nanoscale by self-assembly of enzymes with oppositely charged block polyelectrolytes containing ionic and nonionic water soluble blocks (64,65). The resulting nanoparticles contain a core of protein—polyelectrolyte complex surrounded by a shell of water soluble nonionic polymer such as polyethylene glycol (PEG). In the current work, we immobilized catalase by reacting it with a cationic block copolymer, polyethyleneimine-poly(ethylene glycol) (PEI-PEG), previously used for delivery of polynucleotides (66). The resulting block ionomer complexes of catalase ("nanozymes") are taken up by BMM. We present evidence that such modification protects catalase against degradation in BMM, that BMM release nanozymes in the external medium for at least 4–5 days, and that BMM can carry nanozymes to the brain in the MPTP model of PD.

EXPERIMENTAL PROCEDURES

Materials

Catalase from bovine liver, polyethylenimine (PEI) (2K, branched, 50% aq solution), sulforhodamine-B (SRB), sodium dodecylsulfate (SDS), Sephadex G-25, and Triton X-100 were purchased from Sigma-Aldrich (St-Louis, MO). Meth-oxypoly(ethylene glycol) epoxy (Me-PEG-epoxy) was purchased from Shearwater Polymer Inc., Huntsville, AL (custom synthesis).

BMM

Bone marrow cells extracted from murine femurs (C57BL/6, female mice) as described (32) were cultured for 10 days in the media supplemented with 1000 U/mL macrophage colony-stimulating factor (MCSF) (a generous gift from Wyeth Pharmaceutical, Cambridge, MA). The purity of monocyte culture was determined by flow cytometry using FACSCalibur (BD Biosciences, San Jose, CA).

Microglia

Brains from C57BL/6 neonates (1–3 days old) were removed, washed with ice-cold HBSS, and mashed into small pieces. Supernatant was replaced for 2.5% trypsin and DNAse solution (1 mg/mL) and incubated for 30 min at 37 °C, and then 1 mL of ice cold FBS with 10 mL HBSS was added. The mixture was centrifuged (5 min, 1500 rpm, 4 °C), and complete media with MCSF was added to the pellet. The cells were cultured until maturation (typically 10 days).

MPTP

For MPTP-intoxication recipient C57BL/6, mice were treated as described (67). After 12 h, MPTP-treated mice were injected i.v. with the 50 μCi/mouse of ^{125}I-labeled nanozyme alone or nanozyme loaded into BMM (10×10^6 cells/mouse, 4 mice/group). After 24 h mice were sacrificed and the amount of radioactivity in major organs (brain, spleen, liver, lungs, and kidney) was detected by 1480 gamma-counter Wizard 3 (Perkin-Elmer Life Sciences, Shelton, CT). The amount of the delivered enzyme was expressed as a percent of the injected dose for the whole organ.

PEI-PEG Conjugates

The copolymer was synthesized using a modified procedure (68) by conjugation of PEI and Me-PEG-epoxy. Briefly, Me-PEG-epoxy water solution was added to 5% PEI in water and incubated overnight at RT. To purify from the excess of PEI (as well as from low molecular weight residuals), the obtained conjugates were dialyzed in SpectraPore membrane tubes with cutoff 6000–8000 Da against water (twice replaced) for 48 h and then concentrated *in Vacuo*. For final purification, the conjugate was dissolved in 20 mL of 100% methanol and then added dropwise to 400 mL of ether. The precipitate was centrifuged (400*g*, 5 min), washed twice with ether, and dried in an exicator. Detailed characterization of the product was performed by spectrophotometry and mass spectrometry as reported (68).

Block Ionomer Complexes

Given amounts of the catalase (1 mg/mL) and the block copolymer (2 mg/mL) were separately dissolved in phosphate-buffered saline (PBS) at RT. A solution of the enzyme was added dropwise to the block copolymer solution at constant stirring. The +/- charge ratio (*Z*) was calculated by dividing the amount of amino groups of PEI-PEG protonated at pH 7.4 (66) by the total amount of Gln and Asp in catalase. A combination of physicochemical methods (electrophoretic retention, dynamic light scattering (DLS), and transmission electron microscopy (TEM)) was used to characterize composition, size, dispersion stability, morphology, shape, and structure of the obtained nanoparticles, as described previously (69-72).

Electrophoretic Retention

The formation of polyion complexes was examined by acrylamide gel shift assay. Enzyme complexes at various *Z* were loaded in a 7.5% acrylamide gel with 5 mM Tris, 50 mM glycine, pH 8.3, under nondenaturizing conditions (in the absence of SDS) to preserve the complex. The protein bands were visualized with rabbit polyclonal anti-catalase (Ab 1877, Abcam Inc, Cambridge, MA; 1:6000) and secondary horseradish peroxidase anti-rabbit Ig Ab (Amersham Life Sciences, Cleveland, OH; 1:1500). The specific protein bands were visualized using a chemiluminescence kit (Pierce, Rockford, IL).

Light Scattering Measurements

Effective hydrodynamic diameter and zeta-potential of nanozymes was measured by photon correlation spectroscopy using ‘ZetaPlus’ Zeta Potential Analyzer (Brookhaven Instruments, Santa Barbara, CA) as described previously (73,74).

TEM

A drop of catalase/PEI-PEG dispersion (*Z* = 1) in PBS was placed on Formvar-coated copper grid (150 mesh, Ted Pella Inc., Redding, CA). The dried grid containing nanozymes was stained with vanadyl sulfate and visualized using a Philips 201 transmission electron microscope (Philips/FEI Inc., Briarcliff Manor, NY).

Catalase and Catalase Activity

The activity of the enzyme in polymer nanoparticles (75) was studied using the reaction rate of hydrogen peroxide decomposition by catalase or nanozymes at various charge ratios and was determined by monitoring the change in absorbance at 240 nm (the extinction coefficient of H_2O_2 is 44×10^6 M^{-1} cm^1).

Labeling Catalase with Alexa Fluor 594 and Rhodamine Isothiocyanate (RITC)

For loading and release studies, the enzyme was labeled with Alexa Fluor 594 Protein Labeling Kit (A10239, Molecular probes, Inc., Eugene, OR) according to the manufacturers protocol. For confocal microscopy studies, catalase was labeled with RITC. Briefly, catalase was dissolved in 0.1 M sodium carbonate buffer, pH 8.5 (1 mg/mL), and treated with RITC (10 mg/mL) in DMSO for 2 h at RT. Labeled catalase was purified from low molecular weight residuals by gel filtration on a Sephadex G-25 column (1 × 20 cm) in PBS at elution rate 0.5 mL min^{-1} and lyophilized.

Accumulation and Release of Nanozymes in BMM

BMM grown on 24-well plates (2.5×10^6cells/plate) (76,77) were preincubated with assay buffer (122 mM NaCl, 25 mM $NaHCO_3$, 10 mM glucose, 3 mM KCl, 1.2 mM $MgSO_4$, 0.4 mM K_2HPO_4, 1.4 mM $CaCl_2$, and 10 mM HEPES) for 20 min. Following preincubation, the cells were treated with the Alexa-Fluor 594 labeled enzyme (0.7 mg/mL) in assay buffer alone or nanozyme for various time points. After incubation, the cells were washed three times with ice-cold PBS and solubilized in Triton X 100 (1%). For measures of nanozyme released from BMM, loaded BMM were incubated with fresh media at various time points. Fluorescence in each sample was measured by a Shimadzu RF5000 fluorescent spectrophotometer (λ_{ex} = 580 nm, λ_{em} = 617 nm). The amount of nanozyme was normalized for protein content and expressed in μg of enzyme per mg of the protein for loading experiments and μg enzyme per mL media as mean ± SEM (n = 4).

Intracellular Localization of Nanozymes

Monocytes grown in the chamber slides (77) were exposed to RITC-labeled nanozyme (Z = 1) for 24 h at 37 °C. Following incubation, the cells were fixed in 4% paraformaldehyde and stained with F-actin-specific Oregon Green 488 phalloidin and a nuclear stain, ToPro-3 (Molecular Probes, Inc., Eugene, OR). Labeled cells were examined by a confocal fluorescence microscopic system ACAS-570 (Meridian Instruments, Okimos, MI) with argon ion laser (excitation wavelength, 488 nm) and corresponding filter set. Digital images were obtained using the CCD camera (Photometrics) and Adobe Photoshop software.

Antioxidant Activity Measures

Mature mouse BMM were loaded with the enzyme alone or nanozymes (Z = 1) for 1 h and washed with PBS, and fresh media was added to the cells. Following various time intervals, the media was collected and antioxidant activity of the enzyme released from BMM was assayed by the rate of hydrogen peroxide decomposition.

Ampex Red Dye Fluorescence Assay

Murine microglial cells seeded in 96-well plates (0.1×10^6 cells/well) were either stimulated with tumor necrosis factor alpha (TNF-α) (200 ng/mL) for 48 h or with nitrated alpha-synuclein (N-α-syn) (0.5 μM) to induce ROS production. In parallel, BMM grown in 24-well plates were loaded with “naked” catalase (1 mg/mL) or nanozyme for 1 h and then incubated with Krebs-Ringer buffer (145 mM NaCl, 4.86 mM KCl, 5.5 mM glucose, 5.7 mM NaH_2PO_4, 0.54 mM $CaCl_2$, 1.22 mM $MgCl_2$, pH 7.4) for 2 h to collect catalase released from the cells into the supernatant (Figure 5A). Following incubation, the supernatants collected from BMM loaded with “naked” catalase or nanozyme were supplemented with Ampex Red Dye stock solution (10 U/mL HRP, 10 mM Ampex Red). For N-α-syn stimulation of microglia, supernatants were also supplemented with 0.5 μM aggregated N-α-syn. Obtained solutions were added to the activated microglial cells, and the decomposition of ROS by “naked” catalase or nanozyme was measured by fluorescence at λ_{ex} = 563 nm, λ_{em} = 587 nm. The effect of the supernatants

collected from nonloaded BMM or loaded with PEI-PEG alone on ROS decomposition was evaluated in comparison to the control experiments.

^{125}I-Labeling of Catalase Nanozyme

To obtain ^{125}I-labeled catalase nanozyme, the protein solution in PBS (1 mg/mL) was incubated for 15 min with Na^{125}I (1 mCi) in the presence of IODO-BEADS Iodination Reagent (Pierce, Rockford, IL) and then purified from nonconjugated label using D-salt Desalting Columns (Pierce, Rockford, IL). ^{125}I-labeled catalase (400 μCi/mL, 0.7 mg/mL) was supplemented with PEI-PEG block copolymer (Z = 1) and loaded into mature monocytes (80 × 10^6 BMM in 1 mL of medium) for 2 h at 37 °C. After incubation, the loaded monocytes were washed three times with ice-cold PBS.

Statistical Analysis

For the all experiments, data are presented as the mean ± SEM. Tests for significant differences between the groups were done using one-way ANOVA with multiple comparisons (Fisher's pairwise comparisons) using GraphPad Prism 4.0 (GraphPad software, San Diego, CA). A minimum p value of 0.05 was estimated as the significance level for all tests.

RESULTS

Manufacture and Testing of Nanozymes

Block ionomer complexes spontaneously form by mixing block ionomers with either oppositely charged surfactants or polyelectrolytes (64,78-80). Neutralization of the polyion charges leads to formation of hydrophobic domains, which segregate in aqueous media into a core of polyion complex micelles. Water-soluble nonionic segments of block ionomers (for example, PEG) prevent aggregation and macroscopic phase separation. As a result, these complexes self-assemble into particles of nanoscale size and form stable aqueous dispersions (Figure 1A). Catalase has a net negative charge under physiological conditions. Therefore, the polyion complexes were obtained in phosphate buffer (pH 7.4) by mixing the enzyme (1 mg/mL) and PEI-PEG (2 mg/mL), which is positively charged.

Catalase and PEI-PEG complexes were obtained at various +/- charge ratios (Z = from 0 to 4). They were subjected to electrophoresis under nondenaturizing conditions and then transferred to nitrocellulose membranes. The protein bands were visualized with antibodies to catalase (Figure 1B). The band intensity decreased as the copolymer increased. This suggested that complexes formed that were unable to enter the gel and was confirmed by DLS. Addition of PEI-PEG to catalase solution (1 mg/mL) resulted in particles of nanoscale size with relatively low polydispersity index (about 0.1–0.2), while no particles were detected for catalase alone.

Particle size depended on the charge ratio, ionic strength, and pH (Figure 1, parts C, D, and E). In PBS, the effective diameter increased as the charge ratio increased and then stabilized at ca. 90 to 100 nm at the charge ratio (Z) of 1 and above (Figure 1C). The zeta-potential was increased upon increasing the amount of the block copolymer (Figure 1C). At a constant charge ratio (Z = 1) large aggregates over 600 nm were formed in the absence of salt (Figure 1D). Addition of salt decreased the particle size which stabilized at ca. 90 nm as the NaCl concentration reached 0.15 M. It is likely that large nonequilibrium polyelectrolyte complex aggregates form upon mixing the catalase and PEI-PEG solutions. In the absence of salt these aggregates could not equilibrate and remained "frozen" due to a low rate of polyion interchange (81,82). As salt was added the polyion interchange was accelerated, resulting in formation of small (equilibrium) particles. These particles were stable in an approximate range of pH 7.4 to 11.5 but irreversibly aggregated when pH was decreased below or increased above this range (Figure 1E). Within this range the catalase and PEI-PEG were oppositely charged. The

aggregation of the complexes was linked to protonation and charge inversion of catalase (pI = 6.5) at low or deprotonation of PEI at high pH. Overall, nanozyme particles were stable under physiological pH and ionic strength. Under these conditions the particles were close to spherical (Figure 1D). No changes in the enzymatic activity of catalase were observed at charge ratios used for subsequent cell loading, delivery, and release experiments (Supporting Information, Figure S-1).

Loading of Catalase Nanozymes in BMM

Initially, using the sulforhodamine-B (SRB) cell viability assay, we demonstrated that nanozymes (as well as catalase or copolymer alone) did not induce BMM cytotoxicity over a wide range of concentrations (0.03 to 1000 μg catalase per mL) (Supporting Information, Figure S-2). The accumulation kinetics suggested a rapid uptake of both free catalase and nanozyme in BMM (Figure 2A). Notably the free enzyme was taken up in BMM almost twice as fast as the nanozyme. At 60 min time point the loading of BMM with nanozyme was ca. 30 μg catalase/10^6 cells. The uptake of the nanozyme at the 60 min time point decreased as the charge ratio increased (Figure 2B), which may be due to the effect of the PEG corona. The confocal microscopy data suggested vesicular and/or cytoplasmic localization of RITC-labeled catalase administered to BBM in nanozyme (Figure 2C).

Nanozyme Release from BMM

Mature BMM were pre-loaded with Alexa Fluor 594-labeled catalase nanozyme (60 min) and then cultured in the fresh media for different time intervals. The loaded BMM released catalase in the external media for at least 4–5 days (Figure 3). During the same period, the amount of the enzyme associated with the cells was proportionally decreased. Exposure of nanozyme-loaded BMM to 10 μM phorbol myristate acetate (PMA), a potent activator of the protein kinase C pathway and ROS generation (83), enhanced enzyme release in the media by ca. 50% (Supporting Information, Figure S-3). This suggested that release of nanozyme from BMM may be dependent on cell activation.

BMM Released Nanozyme Activity

BBM loaded with “naked” catalase or nanozyme were placed in a fresh media, and the activity of the enzyme released in the media was determined at different incubation time intervals. Contrary to BMM loaded with free catalase that was practically inactive after the release, the nanozyme-loaded cells released active enzyme for at least 24 h (Figure 4A). The maximal activity of the released enzyme was observed for BMM loaded with nanozyme prepared at the stoichiometric ratio, $Z = 1$ (Figure 4B). All together, this suggests that incorporation of catalase in a block ionomer complex with PEI-PEG results in protection and sustained release of active catalase from BMM.

Modulation of ROS Released by Activated Microglia

To assess the antioxidant capacity of the catalase nanoformulations on microglial ROS production, BMM loaded with “naked’ catalase or nanozyme were incubated for 2 h in Krebs-Ringer buffer, and the reluctant supernatant was then collected and added to TNF-α (200 ng/mL)-stimulated microglial cells. The catalase in the supernatants collected from the catalase- or nanozyme-loaded BMM decomposed hydrogen peroxide by microglia (Figure 5A). A greater effect was observed by nanozyme, which was consistent with its ability to preserve enzyme activity in carrier cells. Furthermore the supernatants collected from unloaded BMM (Figure 5B) or from BMM loaded with PEI-PEG alone (Supporting Information, Figure S-4) had little, if any, effect on the hydrogen peroxide level. To determine whether these findings could be reproduced in microglia activated by stimuli typically found in PD, cells were stimualted with 0.5 μM N-α-syn. Aggregated N-α-syn present as cytoplasmic bodies in PD are

released following the death of dopaminergic neurons and are a major component of Lewy bodies (84) . These aggregated proteins are hypothesized to serve as a stimulus for microglial activation (36, 85). Once again, the level of hydrogen peroxide was significantly reduced with the addition of supernatants from nanozyme loaded BMM (Figure 5C). All together this study suggests that nanozyme released from BMM can attenuate oxidative stress resulting from activation of microglia.

Biodistribution of ^{125}I-labeled Catalase in MPTP-treated Mice

To determine if BMM carrying nanozyme could reach brain subregions with active neuroinflammatory disease reflective of human PD, we used the MPTP model. Two groups of MPTP-intoxicated C57Bl/6 mice were either injected intravenously with free nanozyme containing ^{125}I-labeled catalase or received adoptively transferred nanozyme-loaded BMM. Twenty four hours after injection there were significant increases in the radioactivity levels in spleen, liver, lung, kindney, and brain in the groups receiving adoptive transfer compared to groups treated with nanozyme alone (Figure 6). Noteworthy, after the adoptive transfer about 0.6% of the injected dose was found in the brain which was twice what was found in animals injected with free nanozyme. All together these data provide initial evidence that adoptive transfer of nanozyme loaded BMM can increase the delivery of the enzyme to the brain as well as other peripheral tissues known to be sites of macrophage tissue migration.

DISCUSSION

Efficient transport of therapeutic polypeptides to the brain is required for successful therapies for neurodegenerative and neuroinflammatory diseases. To this end, we examined whether BMM could be used as vehicles for delivery of a potent antioxidant, catalase. Indeed, it has long been known that macrophages and microglia as well as other mononuclear phagocytes can endocytose colloidal nanomaterials, for example, liposomes or nanosuspensions, and subsequently carry and release the drug to site of tissue injury, infection, or disease (32,33, 35,46,86).

Moreover, the abilities of BMM to cross BBB was also investigated (87-94). In particular, it was demonstrated that monocytes infiltrate the brain in the MPTP mouse model of PD (91-93). Indeed, MPTP toxicity stimulated transient and global increases in the rate of monocyte infiltration into the midbrain, stratum, septum, and hippocampus. In these prior studies, the maximal accumulation of the monocyte-macrophages in the brain was observed 1 day after the MPTP treatment. On the basis of these data, we hypothesize that catalase-loaded monocytes adoptively transferred in MPTP-treated mice can deliver enzyme to regions of the brain most affected in PD and including the substantia nigra and striatum.

To protect against catalase degradation inside the BMM, the protein was immobilized in the block ionomer complex with a cationic block copolymer, PEI-PEG. The resulting nanoparticles, nanozymes, were ca. 60 to 100 nm in size and stable in physiological conditions (pH, ionic strength). We optimized the composition and structure of nanozymes to achieve high loading in BMM and preserve catalase activity. Internalization of foreign particles, as well as the exocytotic secretion, is one of the most basic functions in macrophages (95). This study demonstrated that BMM can accumulate a significant amount of nanozyme (ca. 30 μg catalase/10^6 cells) in a relatively short time period (about 40–60 min), followed by its sustained release during 4–5 days into the external media. This also suggested that nanozyme-loaded cells after adoptive transfer may have sufficient time to reach the brain and release catalase. Moreover, it was reported (96-98) that exocytosis can be stimulated by activation of monocytes and macrophages. Our experiment shows that release of nanozyme by BMM can be enhanced by stimulation with PMA.

We also demonstrate that block ionomer complex protects activity of catalase inside the host cells. Notably, the nanozyme-loaded BMM released active enzyme in the media for at least 24 h. Furthermore, the culture supernatants collected from nanozyme-loaded BMM had potent antioxidant effects in our assay for ROS produced by microglia activated with either N-α-syn or TNF-α. Thus, these cell culture models suggest that nanozyme-loaded BMM can mitigate oxidative stress that may be associated with the neurodegenerative process. Finally, we provide initial *in vivo* evidence that adoptive transfer of nanozyme-loaded BMM can increase delivery of labeled enzyme into the tissues including 2-fold increase in the amount of the enzyme in the brain in MPTP-treated mice. Interestingly, considerable amount of the labeled enzyme was also found in the brain after injection of the nanozyme alone. We cannot exclude that in this case the nanozyme may be taken up by circulating monocytes, which then carry the enzyme to the brain. Our further experiments will examine the possibilities for increasing nanozyme transport specifically to the areas of neurodegeneration and evaluate neuroprotective effects in PD models.

Overall, we demonstrate that BMM loaded with catalase incorporated into a protective polymer container and has therapeutic potential. We are cautiously optimistic that these studies will lead to development of new technologies based on cell-mediated delivery of therapeutic polypeptides that can attenuate oxidative stress and elicit anti-inflammatory responses that may be widely useful in the treatment of neurodegenerative disorders.

Supplementary Material

Refer to Web version on PubMed Central for supplementary material.

ACKNOWLEDGMENT

This study was supported by Tobacco Settlement Funds awarded to University of Nebraska, NSF DMR-0071682 to A.V.K. and 2 R37 NS36126, 1 P01 NS043985-01, 5 P01 MH64570-03, and P20 RR15635 to H.E.G. We would like to thank Dr. Sergey Vinogradov for assistance in synthesis of PEI-PEG and Drs. Jonathan Kipnis and Mark Thomas for valuable discussions.

LITERATURE CITED

(1). Brinton RD. A women's health issue: Alzheimer's disease and strategies for maintaining cognitive health. Int. J. Fertil. Womens Med 1999;44:174–85. [PubMed: 10499738]

(2). Gozes I. Neuroprotective peptide drug delivery and development: potential new therapeutics. Trends Neurosci 2001;24:700–5. [PubMed: 11718874]

(3). Kroll RA, Neuwelt EA. Outwitting the blood-brain barrier for therapeutic purposes: osmotic opening and other means. Neurosurgery 1998;42:1083–99. [PubMed: 9588554]discussion 1099–100

(4). Bachis A, Mocchetti I. Brain-Derived Neurotrophic Factor Is Neuroprotective against Human Immunodeficiency Virus-1 Envelope Proteins. Ann. N. Y. Acad. Sci 2005;1053:247–57. [PubMed: 16179530]

(5). Wang, J. Ying; Peruzzi, F.; Lassak, A.; Del Valle, L.; Radhakrishnan, S.; Rappaport, J.; Khalili, K.; Amini, S.; Reiss, K. Neuroprotective effects of IGF-I against TNFalpha-induced neuronal damage in HIV-associated dementia. Virology 2003;305:66–76. [PubMed: 12504542]

(6). Koliatsos VE, Clatterbuck RE, Nauta HJ, Knusel B, Burton LE, Hefti FF, Mobley WC, Price DL. Human nerve growth factor prevents degeneration of basal forebrain cholinergic neurons in primates. Ann. Neurol 1991;30:831–40. [PubMed: 1789695]

(7). Dogrukol-Ak D, Banks WA, Tuncel N, Tuncel M. Passage of vasoactive intestinal peptide across the blood-brain barrier. Peptides 2003;24:437–44. [PubMed: 12732342]

(8). Desnick RJ, Schuchman EH. Enzyme replacement and enhancement therapies: lessons from lysosomal disorders. Nat. ReV. Genet 2002;3:954–66. [PubMed: 12459725]

(9). Urayama A, Grubb JH, Sly WS, Banks WA. Developmentally regulated mannose 6-phosphate receptor-mediated transport of a lysosomal enzyme across the blood-brain barrier. Proc. Natl. Acad. Sci. U.S.A 2004;101:12658–63. [PubMed: 15314220]

(10). Banks W. Is obesity a disease of the blood-brain barrier? Physiological, pathological, and evolutionary considerations. Curr. Pharm. Des 2003;9:801–809. [PubMed: 12678879]

(11). Banks W, Lebel C. Strategies for the delivery of leptin to the CNS. J. Drug Target 2002;10:297–308. [PubMed: 12164378]

(12). Perry VH, Bell MD, Brown HC, Matyszak MK. Inflammation in the nervous system. Curr. Opin. Neurobiol 1995;5:636–41. [PubMed: 8580715]

(13). Prasad KN, Cole WC, Hovland AR, Prasad KC, Nahreini P, Kumar B, Edwards-Prasad J, Andreatta CP. Multiple antioxidants in the prevention and treatment of neurodegenerative disease: analysis of biologic rationale. Curr. Opin. Neurol 1999;12:761–70. [PubMed: 10676761]

(14). McGeer PL, Itagaki S, Boyes BE, McGeer EG. Reactive microglia are positive for HLA-DR in the substantia nigra of Parkinson's and Alzheimer's disease brains. Neurology 1988;38:1285–91. [PubMed: 3399080]

(15). Busciglio J, Yankner BA. Apoptosis and increased generation of reactive oxygen species in Down's syndrome neurons in vitro. Nature 1995;378:776–9. [PubMed: 8524410]

(16). Ebadi M, Srinivasan SK, Baxi MD. Oxidative stress and antioxidant therapy in Parkinson's disease. Prog. Neurobiol 1996;48:1–19. [PubMed: 8830346]

(17). Wu DC, Teismann P, Tieu K, Vila M, Jackson-Lewis V, Ischiropoulos H, Przedborski S. NADPH oxidase mediates oxidative stress in the 1-methyl-4-phenyl-1,2,3,6-tetrahy-dropyridine model of Parkinson's disease. Proc. Natl. Acad. Sci. U.S.A 2003;100:6145–50. [PubMed: 12721370]

(18). Ambani LM, Van Woert MH, Murphy S. Brain peroxidase and catalase in Parkinson disease. Arch. Neurol 1975;32:114–8. [PubMed: 1122174]

(19). Riederer P, Sofic E, Rausch WD, Schmidt B, Reynolds GP, Jellinger K, Youdim MB. Transition metals, ferritin, glutathione, and ascorbic acid in parkinsonian brains. J. Neurochem 1989;52:515–20. [PubMed: 2911028]

(20). Abraham S, Soundararajan CC, Vivekanandhan S, Behari M. Erythrocyte antioxidant enzymes in Parkinson's disease. Indian J. Med. Res 2005;121:111–5. [PubMed: 15756044]

(21). Wu DC, Jackson-Lewis V, Vila M, Tieu K, Teismann P, Vadseth C, Choi DK, Ischiropoulos H, Przedborski S. Blockade of microglial activation is neuroprotective in the 1-methyl-4-phenyl-1,2,3,6-tetrahydropyridine mouse model of Parkinson disease. J. Neurosci 2002;22:1763–71. [PubMed: 11880505]

(22). Du Y, Ma Z, Lin S, Dodel RC, Gao F, Bales KR, Triarhou LC, Chernet E, Perry KW, Nelson DL, Luecke S, Phebus LA, Bymaster FP, Paul SM. Minocycline prevents nigrostriatal dopaminergic neurodegeneration in the MPTP model of Parkinson's disease. Proc. Natl. Acad. Sci. U.S.A 2001;98:14669–74. [PubMed: 11724929]

(23). Kurkowska-Jastrzebska I, Babiuch M, Joniec I, Przybylkowski A, Czlonkowski A, Czlonkowska A. Indomethacin protects against neurodegeneration caused by MPTP intoxication in mice. Int. Immunopharmacol 2002;2:1213–8. [PubMed: 12349958]

(24). Teismann P, Ferger B. Inhibition of the cyclooxy-genase isoenzymes COX-1 and COX-2 provide neuroprotection in the MPTP-mouse model of Parkinson's disease. Synapse 2001;39:167–74. [PubMed: 11180504]

(25). Ferger B, Teismann P, Earl CD, Kuschinsky K, Oertel WH. Salicylate protects against MPTP-induced impairments in dopaminergic neurotransmission at the striatal and nigral level in mice. Naunyn Schmiedebergs Arch. Pharmacol 1999;360:256–61. [PubMed: 10543426]

(26). Ferger B, Spratt C, Earl CD, Teismann P, Oertel WH, Kuschinsky K. Effects of nicotine on hydroxyl free radical formation in vitro and on MPTP-induced neurotoxicity in vivo. Naunyn Schmiedebergs Arch. Pharmacol 1998;358:351–9. [PubMed: 9774223]

(27). Peng J, Stevenson FF, Doctrow SR, Andersen JK. Superoxide dismutase/catalase mimetics are neuroprotective against selective paraquat-mediated dopaminergic neuron death in the substantial nigra: implications for Parkinson disease. J. Biol. Chem 2005;280:29194–8. [PubMed: 15946937]

(28). Gonzalez-Polo RA, Soler G, Rodriguezmartin A, Moran JM, Fuentes JM. Protection against MPP + neurotoxicity in cerebellar granule cells by antioxidants. Cell Biol. Int 2004;28:373–80. [PubMed: 15193280]

(29). Maruyama W, Akao Y, Carrillo MC, Kitani K, Youdium MB, Naoi M. Neuroprotection by propargylamines in Parkinson's disease: suppression of apoptosis and induction of prosurvival genes. Neurotoxicol. Teratol 2002;24:675–82. [PubMed: 12200198]

(30). Group TPS. Effects of tocopherol and deprenyl on the progression of disability in early Parkinson's disease. N. Engl. J 1993;328:176–183.

(31). Pappert EJ, Tangney CC, Goetz CG, Ling ZD, Lipton JW, Stebbins GT, Carvey PM. Alpha-tocopherol in the ventricular cerebrospinal fluid of Parkinson's disease pa-tients: dose-response study and correlations with plasma levels. Neurology 1996;47:1037–42. [PubMed: 8857741]

(32). Dou H, Destache CJ, Morehead JR, Mosley RL, Boska MD, Kingsley J, Gorantla S, Poluektova L, Nelson JA, Chaubal M, Werling J, Kipp J, Rabinow BE, Gendelman HE. Development of a macrophage-based nanoparticle platform for antiretroviral drug delivery. Blood 2006;108:2827–35. [PubMed: 16809617]

(33). Dou H, Morehead JR, Destache C, Kingsley J, Shlyakht-enko L, Zhou Y, Chaubal M, Werling J, Kipp J, Rabinow B, Gendelman H. Laboratory investigations for the morphologic, pharmacokinetic, and anti-retroviral properties of indinavir nanoparticles in human nomocyte-derived macrophages. Virology 2007;358:148–158. [PubMed: 16997345]

(34). Kadiu I, Glanzer JG, Kipnis J, Gendelman HE, Thomas MP. Mononuclear phagocytes in the pathogenesis of neurodegenerative diseases. Neurotox. Res 2005;8:25–50. [PubMed: 16260384]

(35). Gorantla S, Dou H, Boska M, Destache C, Nelson J, Poluektova L, Rabinow B, Gendelman H, Mosley R. Quantitative magnetic resonance and SPECT imaging for macroph-age tissue migration and nanoformulated drug delivery. J. Leukocyte Biol 2006;80:1165–1174. [PubMed: 16908517]

(36). Gendelman H. Synuclein-linked neuroimmunity and the pathogenesis of Parkinson's disease. Neurotoxicology 2006;27:1162–1162.

(37). Mosley R, Benner E, Kadiu I, Thomas M, Boska M, Hasan K, Laurie C, Gendelman H. Neuroinflammation, oxidative stress, and the pathogenesis of Parkinson's disease. Clin. Neurosci. Res 2006;6:261–281. [PubMed: 18060039]

(38). El-Agnaf OM, Salem SA, Paleologou KE, Cooper LJ, Fullwood NJ, Gibson MJ, Curran MD, Court JA, Mann DM, Ikeda S, Cookson MR, Hardy J, Allsop D. Alpha-synuclein implicated in Parkinson's disease is present in extracellular biological fluids, including human plasma. FASEB J 2003;17:1945–7. [PubMed: 14519670]

(39). Anthony DC, Bolton SJ, Fearn S, Perry VH. Age-related effects of interleukin-1 beta on polymorphonuclear neutrophil-dependent increases in blood-brain barrier permeability in rats. Brain 1997;120(Pt 3):435–44. [PubMed: 9126055]

(40). Anthony DC, Blond D, Dempster R, Perry VH. Chemokine targets in acute brain injury and disease. Prog. Brain Res 2001;132:507–24. [PubMed: 11545015]

(41). Blamire AM, Anthony DC, Rajagopalan B, Sibson NR, Perry VH, Styles P. Interleukin-1beta - induced changes in blood-brain barrier permeability, apparent diffusion coefficient, and cerebral blood volume in the rat brain: a magnetic resonance study. J. Neurosci 2000;20:8153–9. [PubMed: 11050138]

(42). Persidsky Y, Ghorpade A, Rasmussen J, Limoges J, Liu XJ, Stins M, Fiala M, Way D, Kim KS, Witte MH, Weinand M, Carhart L, Gendelman HE. Microglial and astrocyte chemokines regulate monocyte migration through the blood-brain barrier in human immunodeficiency virus-1 encephalitis. Am. J. Pathol 1999;155:1599–611. [PubMed: 10550317]

(43). Kuby, J. Immunology. Freeman, WH. and Co.; New York: 1994.

(44). Pawlowski NA, Kaplan G, Abraham E, Cohn ZA. The selective binding and transmigration of monocytes through the junctional complexes of human endothelium. J. Exp. Med 1988;168:1865–82. [PubMed: 3183575]

(45). Lossinsky AS, Shivers RR. Structural pathways for macromolecular and cellular transport across the blood-brain barrier during inflammatory conditions. Review. Histol. Histopathol 2004;19:535–64.

(46). Daleke DL, Hong K, Papahadjopoulos D. Endocytosis of liposomes by macrophages: binding, acidification and leakage of liposomes monitored by a new fluorescence assay. Biochim. Biophys. Acta 1990;1024:352–66. [PubMed: 2162207]

(47). Lee KD, Hong K, Papahadjopoulos D. Recognition of liposomes by cells: in vitro binding and endocytosis mediated by specific lipid headgroups and surface charge density. Biochim. Biophys. Acta 1992;1103:185–97. [PubMed: 1543703]

(48). Nishikawa K, Arai H, Inoue K. Scavenger receptor-mediated uptake and metabolism of lipid vesicles containing acidic phospholipids by mouse peritoneal macrophages. J. Biol. Chem 1990;265:5226–31. [PubMed: 2318890]

(49). Fujiwara M, Baldeschwieler JD, Grubbs RH. Receptor-mediated endocytosis of poly(acrylic acid)-conjugated liposomes by macrophages. Biochim. Biophys. Acta 1996;1278:59–67. [PubMed: 8611608]

(50). Aoki H, Kakinuma K, Morita K, Kato M, Uzuka T, Igor G, Takahashi H, Tanaka R. Therapeutic efficacy of targeting chemotherapy using local hyperthermia and thermosensitive liposome: evaluation of drug distribution in a rat glioma model. Int. J. Hypertherm 2004;20:595–605.

(51). Calvo P, Gouritin B, Chacun H, Desmaele D, D'Angelo J, Noel J, Georgin D, Fattal E, Andreux J, Couvreur P. Long-circulating PEGylated polycyanoacrylate nanoparticles as new drug carrier for brain delivery. Pharm. Res 2001;18:1157–1166. [PubMed: 11587488]

(52). Gref R, Minamitake Y, Peracchia M, Trubetskoy V, Torchilin V, Langer R. Biodegradable long-circulating polymeric nanospheres. Science 1994;263:1600–1603. [PubMed: 8128245]

(53). Harada A, Kataoka K. Chain length recognition: core-shell supramolecular assembly from oppositely charged block copolymers. Science 1999;283:65–7. [PubMed: 9872741]

(54). Jaturanpinyo M, Harada A, Yuan X, Kataoka K. Preparation of bionanoreactor based on core-shell structured polyion complex micelles entrapping trypsin in the core cross-linked with glutaraldehyde. Bioconjugate Chem 2004;15:344–8.

(55). Kabanov A, Batrakova E, Alakhov V. Pluronic block copolymers as novel polymer therapeutics for drug and gene delivery. J. Controlled Release 2002;82:189–212.

(56). Kwon GS. Polymeric micelles for delivery of poorly water-soluble compounds. Crit. ReV. Ther. Drug Carrier Syst 2003;20:357–403. [PubMed: 14959789]

(57). Mora M, Sagrista ML, Trombetta D, Bonina FP, De Pasquale A, Saija A. Design and characterization of liposomes containing long-chain N-acylPEs for brain delivery: penetration of liposomes incorporating GM1 into the rat brain. Pharm. Res 2002;19:1430–8. [PubMed: 12425459]

(58). Rousseau V, Denizot B, Le Jeune JJ, Jallet P. Early detection of liposome brain localization in rat experimental allergic encephalomyelitis. Exp. Brain Res 1999;125:255–64. [PubMed: 10229016]

(59). Torchilin VP. Drug targeting. Eur. J. Pharm. Sci 2000;11(Suppl 2):S81–91. [PubMed: 11033430]

(60). Vinogradov SV, Batrakova EV, Kabanov AV. Nanogels for oligonucleotide delivery to the brain. Bioconjugate Chem 2004;15:50–60.

(61). Kabanov VA, Evdakov VP, Mustafaev MI, Antipina AD. A cooperative interaction of serum albumin with quaternized poly-4-vinyl pyridine and structure of the complexes. Mol. Biol. (Russian) 1977;11:582–596.

(62). Kabanov V. Physicochemical basis and the prospects of using soluble interpolyelectrolyte complexes. Polym. Sci 1994;36:183–197.

(63). Kabanov V, Skobeleva V, Rogacheva V, Zezin A. Sorption of proteins by slightly cross-linked polyelectrolyte hydro-gels: Kinetics and mechanism. J. Phys. Chem. B 2004;108:1485–1490.

(64). Harada A, Kataoka K. Pronounced activity of enzymes through the incorporation into the core of polyion complex micelles made from charged block copolymers. J. Controlled Release 2001;72:85–91.

(65). Harada A, Kataoka K. Switching by pulse electric field of the elevated enzymatic reaction in the core of polyion complex micelles. J. Am. Chem. Soc 2003;125:15306–7. [PubMed: 14664571]

(66). Vinogradov S, Bronich T, Kabanov A. Self-assembly of polyamine-poly(ethylene glycol) copolymers with phosphorothioate oligonucleotides. Bioconjugate Chem 1998;9:805–812.

(67). Benner EJ, Mosley RL, Destache CJ, Lewis TB, Jackson-Lewis V, Gorantla S, Nemachek C, Green SR, Przedborski S, Gendelman HE. Therapeutic im-munization protects dopaminergic neurons in

a mouse model of Parkinson's disease. Proc. Natl. Acad. Sci. U.S.A 2004;101:9435–40. [PubMed: 15197276]

(68). Nguyen HK, Lemieux P, Vinogradov SV, Gebhart CL, Guerin N, Paradis G, Bronich TK, Alakhov VY, Kabanov AV. Evaluation of polyether-polyethyleneimine graft copolymers as gene transfer agents. Gene Ther 2000;7:126–38. [PubMed: 10673718]

(69). Vinogradov S, Batrakova E, Li S, Kabanov A. Polyion complex micelles with protein-modified corona for receptor-mediated delivery of oligonucleotides into cells. Bioconjugate Chem 1999;10:851–60.

(70). Lemieux P, Vinogradov SV, Gebhart CL, Guerin N, Paradis G, Nguyen HK, Ochietti B, Suzdaltseva YG, Bartakova EV, Bronich TK, St-Pierre Y, Alakhov VY, Kabanov AV. Block and graft copolymers and NanoGel copolymer networks for DNA delivery into cell. J. Drug Target 2000;8:91–105. [PubMed: 10852341]

(71). Vinogradov SV, Batrakova EV, Li S, Kabanov AV. Mixed polymer micelles of amphiphilic and cationic copoly-mers for delivery of antisense oligonucleotides. J. Drug Target 2004;12:517–26. [PubMed: 15621677]

(72). Vinogradov SV, Zeman AD, Batrakova EV, Kabanov AV. Polyplex Nanogel formulations for drug delivery of cytotoxic nucleoside analogs. J. Controlled Release 2005;107:143–57.

(73). Bronich T, Nguyen H, Eisenberg A, Kabanov A. Recognition of DNA topology in reactions between plasmid DNA and cationic copolymers. J. Am. Chem. Soc 2000;122:8339–8343.

(74). Vinogradov S, Batrakova E, Kabanov A. Poly-(ethylene glycol)-polyethyleneimine NanoGel (TM) particles: novel drug delivery systems for antisense oligonucleotides. Colloids Surf. B-Biointerfaces 1999;16:291–304.

(75). Beckman JS, Minor RL Jr. White CW, Repine JE, Rosen GM, Freeman BA. Superoxide dismutase and catalase conjugated to polyethylene glycol increases endothelial enzyme activity and oxidant resistance. J. Biol. Chem 1988;263:6884–92. [PubMed: 3129432]

(76). Batrakova E, Han H, Miller D, Kabanov A. Effects of pluronic P85 unimers and micelles on drug permeability in polarized BBMEC and Caco-2 cells. Pharm. Res 1998;15:1525–1532. [PubMed: 9794493]

(77). Batrakova EV, Vinogradov SV, Robinson SM, Niehoff ML, Banks WA, Kabanov AV. Polypeptide point modifications with fatty acid and amphiphilic block copolymers for enhanced brain delivery. Bioconjugate Chem 2005;16:793–802.

(78). Kabanov A, Vinogradov S, Suzdaltseva Y, Alakhov V. Water-soluble block polycations as carriers for olygonucle-otide delivery. Bioconjugate Chem 1995;6:639–643.

(79). Harada A, Kataoka K. Formation of polyion complex micelles in an aqueous milieu from a pair of oppositely charged block-copolymers with poly(ethylene glycol) segments. Macromolecules 1995;28:5294–5299.

(80). Bronich T, Kabanov A, Kabanov V, Yu K, Eisenberg A. Soluble complexes from poly(ethylene oxide)-block-polymethacrylate anions and N-alkylpyridinium cations. Macromolecules 1997;30:3519–3525.

(81). Kabanov V. Physicochemical basis and the prospects of using soluble interpolyelectrolyte complexes. Polym. Sci 1994;36:143–156.

(82). Kabanov, V. Fundamentals of Polyelectrolyte Complexes in Solution and the Bulk. In: Decher, G.; Schlenoff, J., editors. Multilayer Thin Films. Wiley-VCH Verlag GmbH & Co.; KGaA, Weinheim: 2003. p. 47-86.

(83). Chang Z, Beezhold D. Protein-kinase-C activation in human monocytes -regulation of PKC isoforms. Immunology 1993;80:360–366. [PubMed: 8288312]

(84). Zhang W, Wang T, Pei Z, Miller DS, Wu X, Block ML, Wilson B, Zhou Y, Hong JS, Zhang J. Aggregated alpha-synuclein activates microglia: a process leading to disease progression in Parkinson's disease. FASEB J 2005;19:533–42. [PubMed: 15791003]

(85). Thomas MP, Chartrand K, Reynolds A, Vitvitsky V, Banerjee R, Gendelman HE. Ion channel blockade attenuates aggregated alpha synuclein induction of microglial reactive oxygen species: relevance for the pathogenesis of Parkinson's disease. J. Neurochem 2007;100:503–19. [PubMed: 17241161]

(86). Jain S, Mishra V, Singh P, Dubey PK, Saraf DK, Vyas SP. RGD-anchored magnetic liposomes for monocytes/neutrophils-mediated brain targeting. Int. J. Pharm 2003;261:43–55. [PubMed: 12878394]

(87). Lawson LJ, Perry VH, Gordon S. Turnover of resident microglia in the normal adult mouse brain. Neuroscience 1992;48:405–15. [PubMed: 1603325]

(88). Simard AR, Rivest S. Bone marrow stem cells have the ability to populate the entire central nervous system into fully differentiated parenchymal microglia. FASEB J 2004;18:998–1000. [PubMed: 15084516]

(89). Male D, Rezaie P. Colonisation of the human central nervous system by microglia: the roles of chemokines and vascular adhesion molecules. Prog. Brain Res 2001;132:81–93. [PubMed: 11545033]

(90). Streit WJ, Walter SA, Pennell NA. Reactive microgliosis. Prog. Neurobiol 1999;57:563–81. [PubMed: 10221782]

(91). Kokovay E, Cunningham LA. Bone marrow-derived microglia contribute to the neuroinflammatory response and express iNOS in the MPTP mouse model of Parkinson's disease. Neurobiol. Dis 2005;19:471–8. [PubMed: 16023589]

(92). Kurkowska-Jastrzebska I, Wronska A, Kohutnicka M, Czlonkowski A, Czlonkowska A. MHC class II positive microglia and lymphocytic infiltration are present in the substantia nigra and striatum in mouse model of Parkinson's disease. Acta Neurobiol. Exp. (Wars) 1999;59:1–8. [PubMed: 10230070]

(93). Kurkowska-Jastrzebska I, Wronska A, Kohutnicka M, Czlonkowski A, Czlonkowska A. The inflammatory reaction following 1-methyl-4-phenyl-1,2,3, 6-tetrahydropyridine intoxication in mouse. Exp. Neurol 1999;156:50–61. [PubMed: 10192776]

(94). Simard AR, Rivest S. Neuroprotective properties of the innate immune system and bone marrow stem cells in Alzheimer's disease. Mol. Psychiatry 2006;11:327–35. [PubMed: 16491130]

(95). Stout RD, Suttles J. T cell signaling of macrophage function in inflammatory disease. Front. Biosci 1997;2:d197–206. [PubMed: 9206987]

(96). Schorlemmer HU, Edwards JH, Davies P, Allison AC. Macrophage responses to mouldy hay dust, Micropolyspora faeni and zymosan, activators of complement by the alternative pathway. Clin. Exp. Immunol 1977;27:198–207. [PubMed: 849651]

(97). Allison AC, Davies P. Mechanisms of endocytosis and exocytosis. Symp. Soc. Exp. Biol 1974:419–46. [PubMed: 4616399]

(98). Cardella CJ, Davies P, Allison AC. Immune complexes induce selective release of lysosomal hydrolases from macrophages. Nature 1974;247:46–8. [PubMed: 4808940]

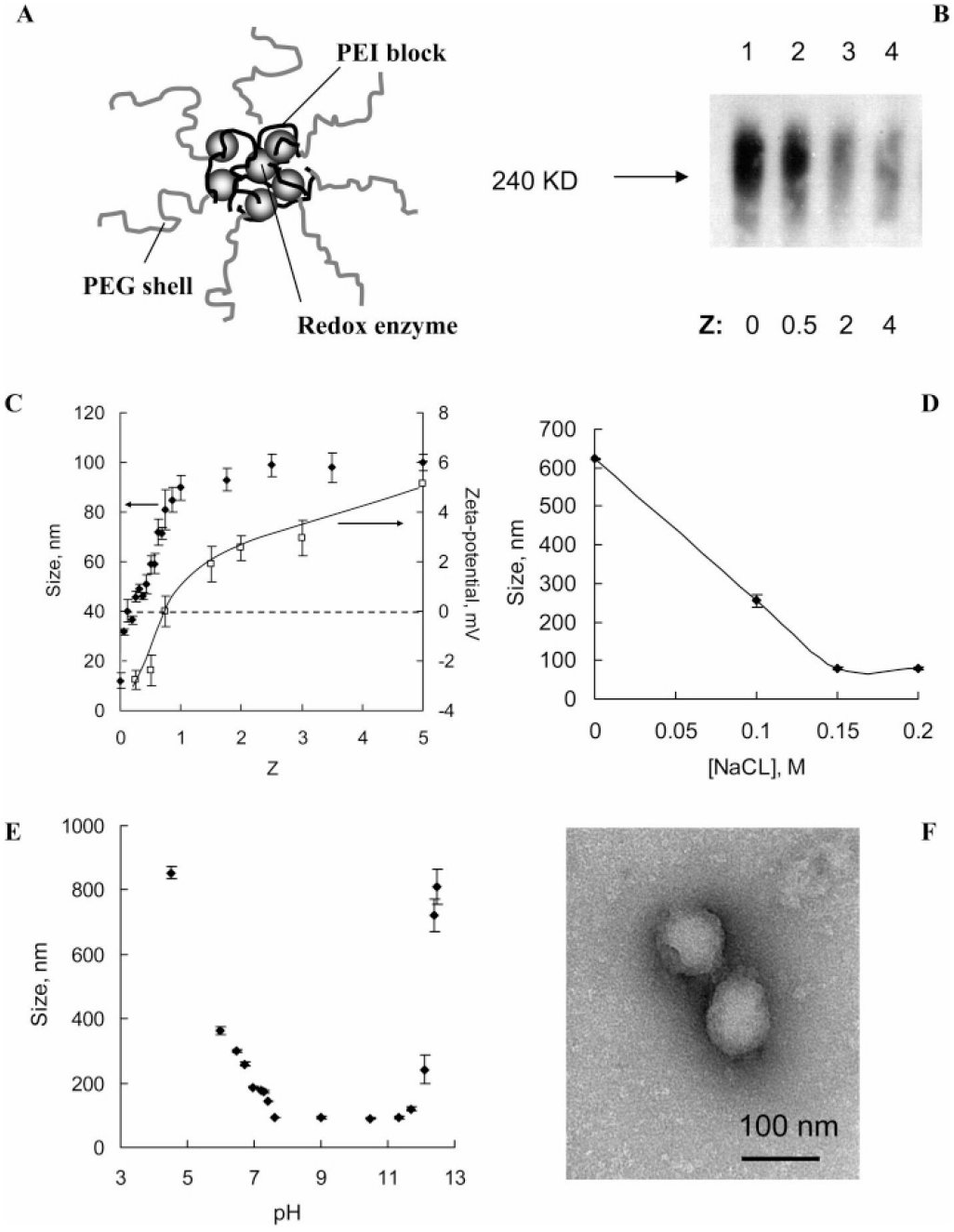

Figure 1.

Characterization of catalase nanozyme. A: Schematic presentation of the enzyme-polyion complex structure. B: Gel retardation assay of the enzyme/polyion complexes at various Z. Samples were subjected to gel electrophoresis in polyacrylamide gel (7.5%) under nondenaturing conditions (without SDS). Line 1: enzyme alone; lines 2–4: enzyme/PEI-PEG complexes with progressive increasing of *Z* (0.5, 2, 4). C—E: Characterization of catalase/polyion complex by DLS. Changes in cumulant diameter (C—E) and zeta-potential (C) of catalase nanozyme with various: C: *Z* in PBS solutions; D: ionic strength (*Z* = 1, pH 7.4); E: pH (*Z* = 1, [NaCl] = 0.15M). F: TEM images of catalase nanozyme (*Z* = 1). Bar represents 100 nm.

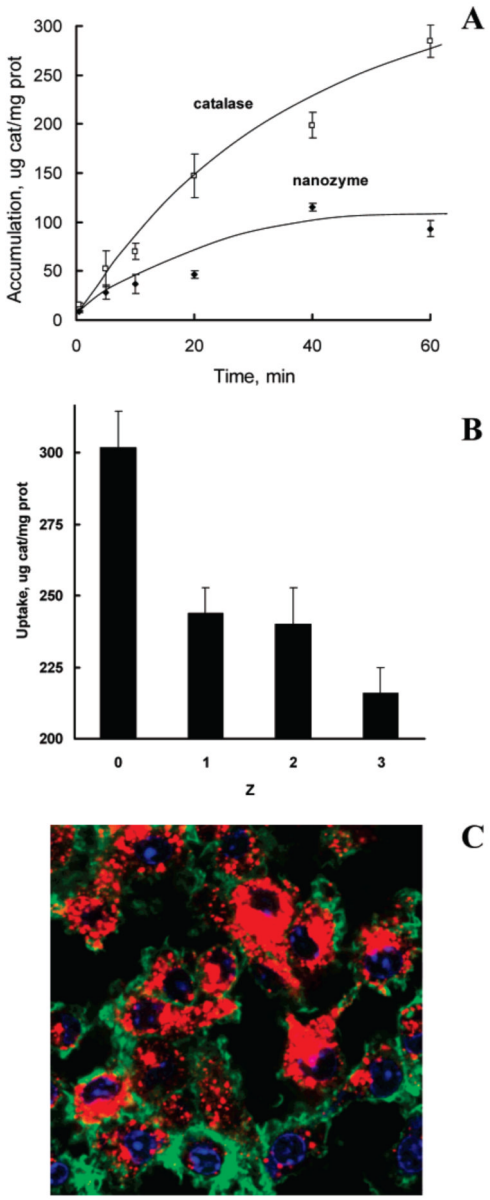

Figure 2.

A: Kinetics of "naked" catalase and nanozyme ($Z = 1$) accumulation in monocytes. Cells were treated with the Alexa Fluor 594 labeled enzyme or nanozyme at various time points. Following incubation, the cellular content was collected, and the amount of fluorescence was measured by fluorescent spectrophotometer ($\lambda_{ex} = 580$ nm, $\lambda_{em} = 617$ nm). Data represent means ± SEM ($n = 4$); B: Accumulation of catalase nanozymes in BMM at various Z. C: Intracellular localization of RITC-labeled catalase nanozyme in BMM. Cells grown on cover slips were loaded with catalase/PEI-PEG complex ($Z = 1$) (red staining) for 24 h. Following the incubation, the cells were fixed and stained with F-actin—specific Oregon Green 488 phalloidin (green) and a nuclear stain, ToPro-3 (blue). Images were obtained by confocal fluorescence microscopic system ACAS-570.

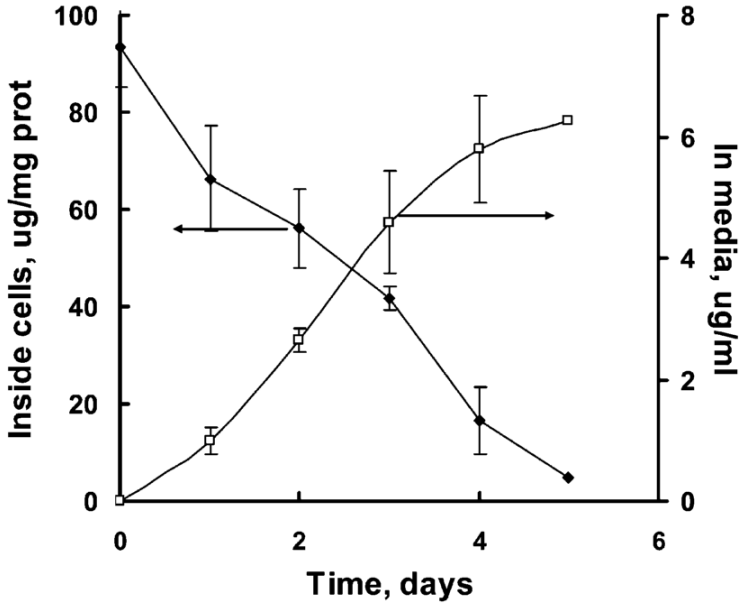

Figure 3.

Release profile of catalase nanozyme from BMM. Cells were loaded with catalase/PEI-PEG complex ($Z = 1$) for 1 h, washed with PBS, and incubated with catalase-free media for various time intervals. Amount of catalase released into the media and retained in the cells was accounted by fluorescent spectrophotometry. Data represent means ± SEM ($n = 4$).

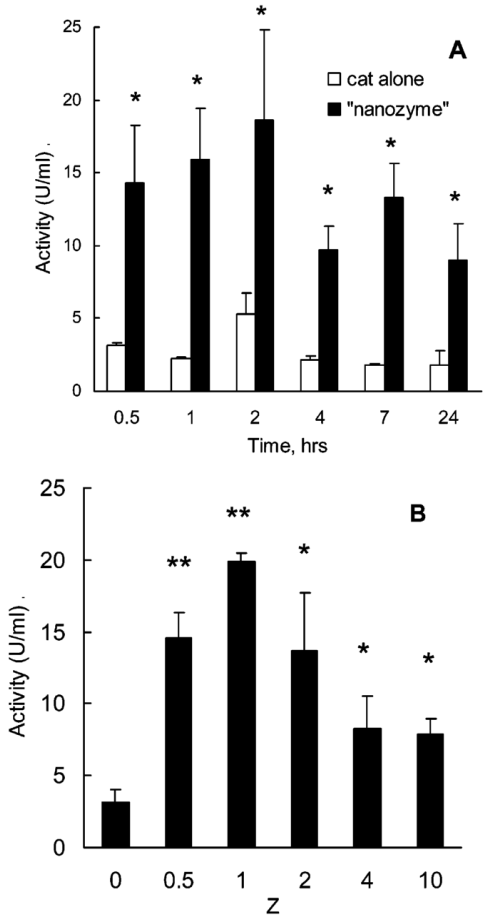

Figure 4.

Preservation of enzymatic activity of catalase against degradation in BMM. A: "Naked" catalase or nanozyme ($Z = 1$) were loaded into BMM, and cells were washed and incubated with catalase-free media for various time intervals. The activity of catalase released from BMM was determined by spectrophotometry. B: Catalase polyion complexes with various compositions (Z) were loaded into the cells and incubated in catalase-free media for 2 h. Then, the media was collected and assessed for catalase activity by spectrophotometry. Data represent means ± SEM ($n = 4$). Statistical significance of nanozyme activity compared to catalase alone is shown by asterisks: (*) $p < 0.05$, (**) $p < 0.005$.

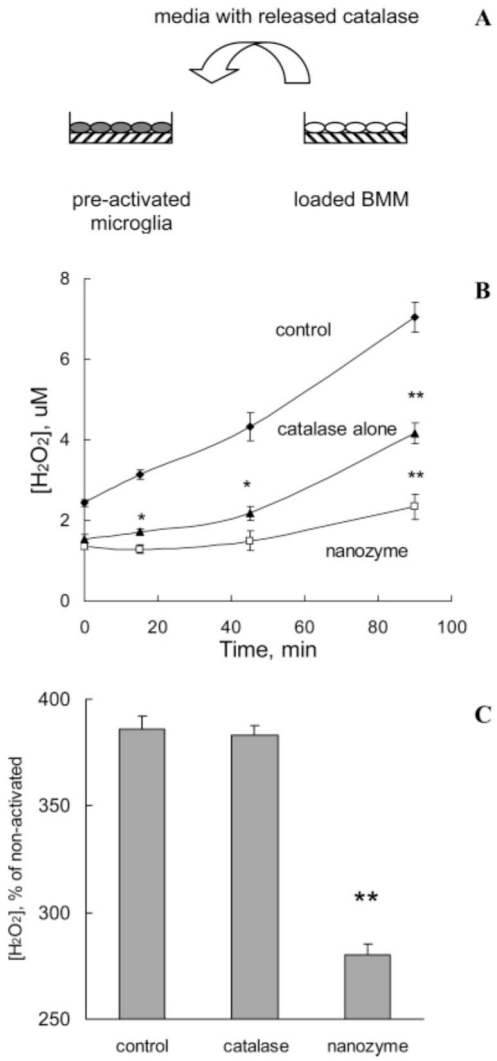

Figure 5.

Modulation of microglial-derived ROS by catalase nanozyme released from BMM (A: overall scheme). "Naked" catalase or catalase nanozyme ($Z = 1$) were loaded into BMM. Then, cells were washed and incubated in Kreb's Ringer buffer for 2 h. In parallel, murine microglial cells were either stimulated with (B) 200 ng/mL TNF-α (48 h), or (C) 0.5 μM N-α-syn. Then, supernatants collected from BMM with the released enzyme were supplemented with Amplex Red and HRP solutions and added to the activated microglial cells. Control activated microglia was incubated with fresh media (B) or 0.5 μM aggregated N-α-syn (C). The amount of H_2O_2 produced by microglial cells and decomposed by catalase released from BMM was detected by fluorescence. Data represent mean ± SEM ($n = 6$). Statistical significance of the amount of H_2O_2 decomposed by released from BMM nanozyme or catalase, compared to activated microglia (control) is shown by asterisks: (*) $p < 0.05$, (**) $p < 0.005$.

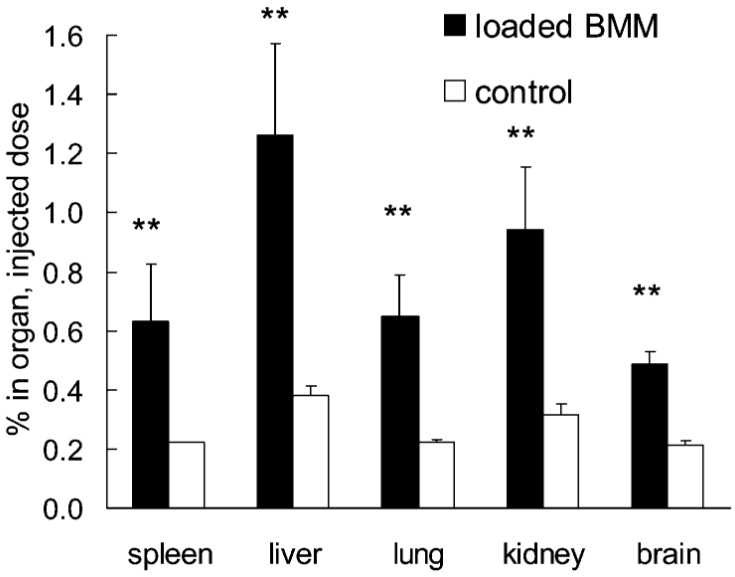

Figure 6.

Biodistribution of ^{125}I-labeled nanozyme in MPTP-treated mice. Mice were injected with BMM (10×10^6 cells/mouse) loaded with catalase nanozyme ($Z = 1$, 50 μCi/mouse) or with nanozyme alone (control group). Twenty-four hours later mice were sacrificed and the amount of radioactivity was measured in various organs. Data represent mean ± SEM ($n = 4$). Statistical significance of the BMM-loaded nanozyme transport compared to the nanozyme alone group is shown by asterisks: (**) $p < 0.005$.